# Development of Sodium Acetate Trihydrate-Ethylene Glycol Composite Phase PCMs with Enhanced Thermal Properties for Thermal Comfort and Therapeutic Applications

## 6.1. INTRODUCTION

The extreme low environmental temperature conditions badly affect the health of residents and may cause hypothermia, frostbite, etc. Physiological alterations in the vital organs like brain, digestive and respiratory system may also occur due to the prolonged exposure to the very low temperature. Therefore, it is essential to provide the preferred thermal environments, using other heating source under such situations for alleviating these problems. At present, hot water bottles, insulating blankets, electric heating blankets/ pads etc. are being utilized to improve comfort in such hostile conditions [Susan and William, 1976]. Insulating blankets provide relief by decreasing the heat transfer rate between environment and body. Though, it does not contain any heating source and therefore may not be appropriate for longer exposures. Hot water bottles delivers primary heating at higher temperatures, which reduces quickly to the lower temperatures because of low thermal energy storage density of water. Therefore, it provides solution for smaller time intervals. The temperature of electrically powered heating devices, such as blankets, pads, etc. is controlled via thermostat and can lead to causalities such as skin burn in the case of failure. In addition, such devices are not appropriate for field applications, where electrical sources are difficult to deal with. In countries like India, residents are using Kangaries as external heating source to warm the body during outdoor activities in high altitude areas such as Kashmir, Leh and Laddakh. Kangaries are not good for health due to release of the poisonous gases e.g. carbon mono/dioxide through coal burning. Simultaneously, skin burning incidents and skin cancer are also possible while using these Kangaries [Imtiaz, 2010]. Bukharies are used for indoor heating and are also not good for health due the release of hazardous gases while burning kerosene as a fuel [Joseph, 2002].

Therefore, unconventional renewable, recyclable and low cost heating systems are required to provide thermal comfort in such conditions. These unconventional heating systems should be self-reliant to store existing thermal energy such as waste heat, solar energy etc. at higher temperature (~60 °C), preserve it at low ambient temperatures and discharge heat later whenever required. The development and effectiveness of such unconventional heating sources will depend on thermophysical properties of heat storing substance such as high TES density and proper heat releasing temperature with a probability of required time deferment between storage and supply of heat. Phase change materials (PCMs) can be useful for such sources because of its desired thermophysical properties. In addition, PCMs store/liberate heat in a very narrow temperature window [Lane, 1983; Abhat, 1983; Zalba *et al.*, 2003; Atul *et al.*, 2009]. Therefore, PCMs have attracted attention towards the development of thermal controlling devices/systems for human body temperature regulation and reduction of indoor temperature variations inside a building [Ulman and Valentin, 1983; Khudhair and Farid, 2004; Haralad Mehling and Cabeza, 2008; Sharma *et al.*, 2009; Gil *et al.*, 2010; Oro *et al.*, 2010].

The hydrated salts based PCMs exhibit large degree of supercooling, which is not appropriate for common heat storage applications such as building heating and cooling etc. Though, this characteristic can be used for long term thermal energy storage at low ambient temperature, which can be utilized later whenever required [Barrett *et al.*, 1984; Barret and Best, 1985]. Among these hydrated PCMs, Sodium Acetate Trihydrate (SAT) has attracted attention because of its high latent heat of fusion ~270 kJ kg$^{-1}$, suitable melting temperature ~ 58 $^{\circ}$C, large supercooling range, better thermal stability during charging and discharging cycles and the most important, low price [Pebler, 1975; Takes, 1980; Wada *et al.*, 1983; Araki *et al.*, 1985; Hiroshi and Junjiro, 1985; Guion and Teisseire, 1991]. Such superior thermophysical properties and low price of SAT make it appropriate for reusable PCM based heating devices such as heat packs, and shelter/building heating and seasonal solar energy storage applications. The reusable PCM based heat packs are being used for body warming to get relief while field operations in cold regions and therapeutic applications such as treatment of hypothermia, frostbite, and muscle aches. These heat packs consist of aqueous SAT solution and metallic strip made of stainless steel (SS) [Kapralis *et al.*, 1990]. The aqueous SAT maintains metastable supercooled liquid state upto ambient temperature or even lower. This metastable state assists in storing latent heat as thermal energy down to ~ 0 $^{\circ}$C for extended time spans [Mansel *et al.* 2003; Sandnes and Raskad, 2006;].

In spite of these outstanding thermophysical properties of SAT and potential uses in heating devices as described schematically in Figure 6.1.
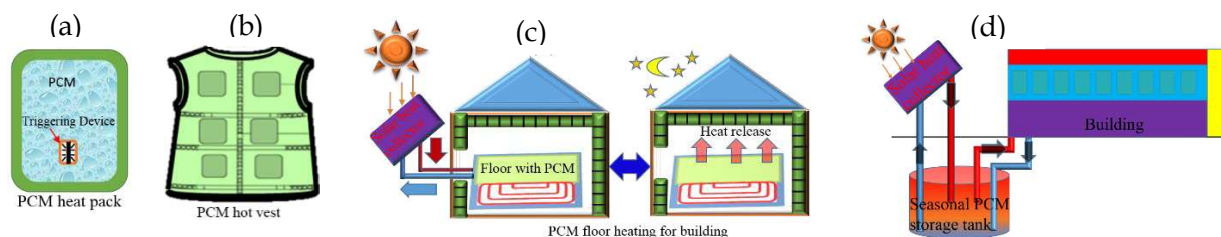


**Figure 6.1:** Schematic representation for use of sodium acetate trihydrate PCM (a) reusable PCM heat pack, (b) PCM hot vest, (c) PCM floor heating for buildings and (d) seasonal solar thermal energy storage and building heating.

There are some issues and challenges related with SAT heat packs such as lumped, hard, big and sharp edges of SAT crystallites, unintended nucleation in metastable supercooled liquid PCM (MSLPCM) at low temperatures (~0 $^{\circ}$C), and short heat retaining time because of fast crystal growth during solidification. These heat packs liberate heat at ~58 $^{\circ}$C, which restricts its applications for diverse applications such as instantaneous heating of tissues after frostbite, where heating at ~40 $^{\circ}$C is essential. The lumped and hard SAT crystallites restrict the shape adaptability of these heating packs as per requirements. The sharp SAT crystallite edges are also inclined to damage/puncture the packaging material and also source of human body discomfort while therapeutic applications. Various reports are available on SAT and SAT based binary eutectics for thermal energy storage applications [Takahiro *et al.*, 1984; Wada *et al.*, 1984; Wada and Matsuo, 1984; Jing-Hua Li *et al.*, 1991; Cabeza *et al.*, 2003; Hu *et al.*, 2011;]. Nevertheless, less-efforts are made to alleviate above discussed limitations for SAT. We investigated thermophysical and microstructural properties of aqueous SAT and SAT-EG composite materials to improve SAT thermophysical properties. We observed that ethylene glycol (EG) helps in reducing aqueous SAT crystallites size and increases the effective heat retention time about 10% with respect to aqueous SAT phase change material. We will discuss the observed thermophysical properties of investigated materials using structural, microstructural,

thermal characterizations and the microscopic origin of enhanced thermal properties of aqueous SAT-EG composite PCMs.

## 6.2 EXPERIMENTAL DETAILS

SAT and EG grade "excel R" are procured from Qualigens Fine Chemicals Pvt. Ltd. Mumbai, India and used without any further purification. The six samples, sample A (94 % SAT + 6 % deionized water), sample B (sample A + 2% EG), sample C (sample A + 3% EG), sample D (sample A + 5% EG), sample E (sample A + 7% EG) and sample F (sample A + 10% EG) are made using physical mixing technique. The samples are homogenized by continuous magnetic stirring of the materials for 20 minutes in liquid phase at 70 ℃. The additional deionized (DI) water is added to the pristine SAT to further improve its cycling thermal stability.

The structural, microstructural and molecular interaction properties of these samples are investigated using X-ray, SEM and FTIR techniques as discussed in earlier chapters. Thermophysical properties of samples are estimated using T-history and DSC techniques. The details about the same is discussed in Chapter 4 and Kumar et al., 2017.

## 6.3. RESULTS AND DISCUSSION

### 6.3.1 X-ray Diffraction Analysis
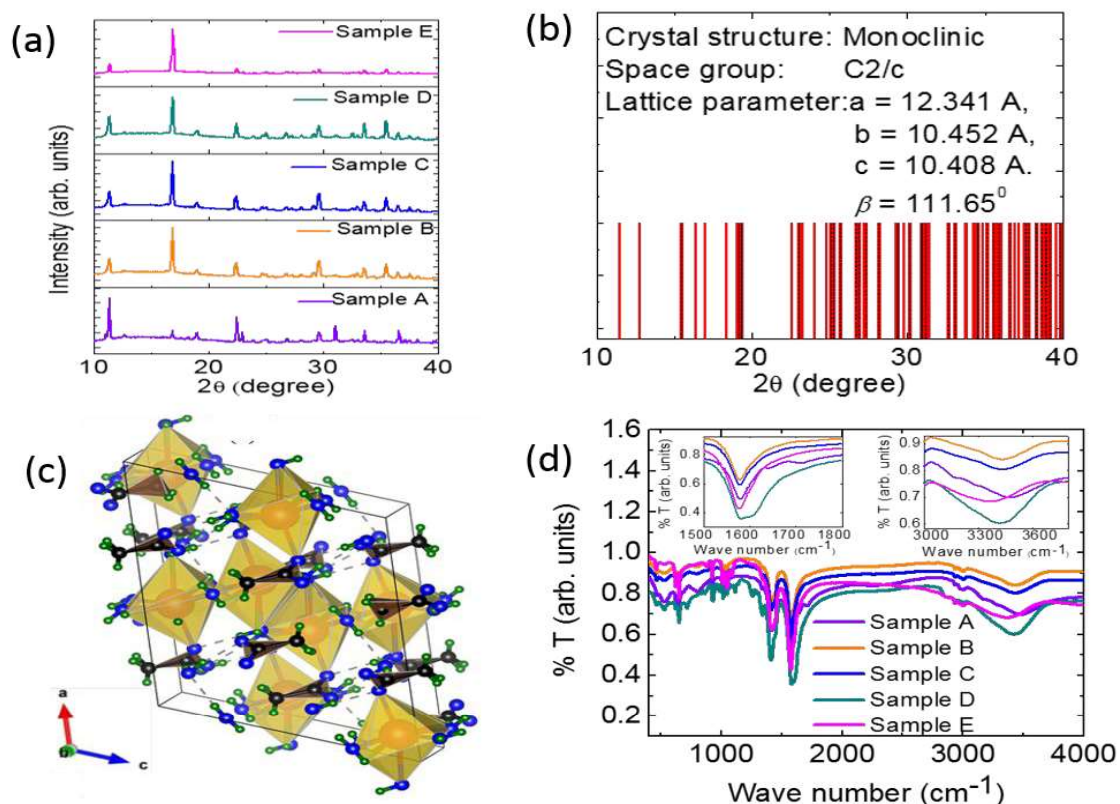


**Figure 6.2:** (a) Measured powder X-ray diffractographs for samples A, B, C, D and E, (b) calculated X-ray diffraction pattern with inset showing lattice parameters, (c) crystal structure of SAT crystal with Orange large sphere: Na atom; blue smaller circle: Oxygen atom, green smaller circle: hydrogen atom, black circle: carbon atom and (d) FTIR spectrographs of sample A, B, C, D and E.

The crystal structure of aqueous SAT (sample A) and EG modified SAT samples B, C, D, and E are investigated using powder X-ray diffraction (pXRD) measurements in $10^o$ – $40^o$ $2\Theta$ range and results are summarized in Figure 6.2(a). The XRD pattern of pristine SAT is in good agreement with the reported monoclinic crystallographic structure with C2/c space group [Cameron *et al.*, 2006]. This is used to calculate the lattice parameters and calculated values are in agreement with the reported literature [Cameron *et al.*, 2006]. The theoretical XRD pattern has been calculated for monoclinic structure (space group C2/c) using the estimated lattice parameters. The generated pattern is summarized in Figure 6.2(b) and observed that generated structure pattern exhibits only those (h k l) diffraction patterns for which h+k = 2n; (h 0 l) with h = 2n, l=2n and (0 k 0) with k = 2n (n is an integer) [Efremov *et al.*, 1986]. These diffraction patterns substantiate the observed C2/c space group for SAT. The crystallographic structure of SAT has been generated using these structural parameters and is shown in Figure 6.2(c) with polyhedron around sodium atom. These edge shared polyhedrons form long chains, may be responsible for long needle shaped crystals as observed in microscopic studies and discussed later. The XRD pattern for EG modified SAT samples (sample C, D and E) are identical to the SAT sample. However, the relative intensity of these diffraction patterns has reduced with increase in EG wt% ratio. The reduced intensity is attributed to the geometrical effects, where smaller crystals have resulted in out of phase diffracted radiation, and thus, showed relatively lower intensity. This has been substantiated with our microscopic observations, discussed later.

## 6.3.2 Fourier Transform Infrared Spectroscopic Analysis

The room temperature Fourier Transform Infrared (FTIR) spectroscopic measurements are carried out on samples A, B, C, D and E. The respective spectrographs are shown in Figure 6.2(d). The respective -OH bending vibrations (1500-1800 cm$^{-1}$) and -OH stretching vibrations (3000-3800 cm$^{-1}$) of $H_2O$ in SAT-EG composite systems are shown in as insets of Figure 6.2(d). These insets suggest that -OH bending and stretching vibrational frequencies shift towards higher and lower frequencies with increasing wt% of EG in aqueous SAT-EG composite materials respectively. The shifting of vibrational frequencies in FTIR vibrational spectra suggests that there are hydrogen bond interactions between H atoms of water and hydroxyl oxygen atoms of ethylene glycol [Zhang *et al.*, 2008]. The observed interaction between H (SAT) – OH (EG) may assist in reducing the melting temperature and increasing the supercooling temperature of aqueous SAT-EG composites against the pristine SAT phase change material.

## 6.3.3 Scanning Electron Microscopic Analysis

The microstructural properties of samples A, B, C, D and E are investigated using SEM and respective micrographs are summarized in Figure 6.3(a - e) and Figure 6.3(f - j) at 500 x and 15k x magnifications, respectively. Figure 6.3(a) explains the sharp and big SAT crystallites, which are substantiated by the pXRD observations with relatively large diffraction intensity (Figure 6.2(a)), as explained above. The sharp and big crystals reduce the shape adaptability and flexibility of heat packs as per requirements. The SEM micrographs shown in Figure 6.3(b, c, d and e) explain the reduction in size and edge sharpness of aqueous SAT crystallites with increasing wt% of EG. These results are in good agreement with pXRD results (Figure 6.2(a)), where the reduced intensity and enhanced FWHM are observed for samples B, C, D, and E with respect to sample A. This reduction in the diffraction intensity suggests that long range ordered crystallite phase (Figure 6.3(a)), has converted into short range ordered microstructures (Figure 6.3(b, c, d and e)). The SEM micrograph of sample A (Figure 6.3(f)), explains the tightly packed crystallites, which are strong and difficult to break into smaller crystallites. Figure 6.3(g - j) explains the insertion of liquid EG into aqueous SAT crystallites during crystal growth, thus, weakening the crystals and assisting the reduction of

crystallite size. The increasing EG wt% in aqueous SAT has led to the enhanced insertion of EG and thus, reducing the crystallite size into micro/nano crystallites, as explained in Figure 6.3(g - j).
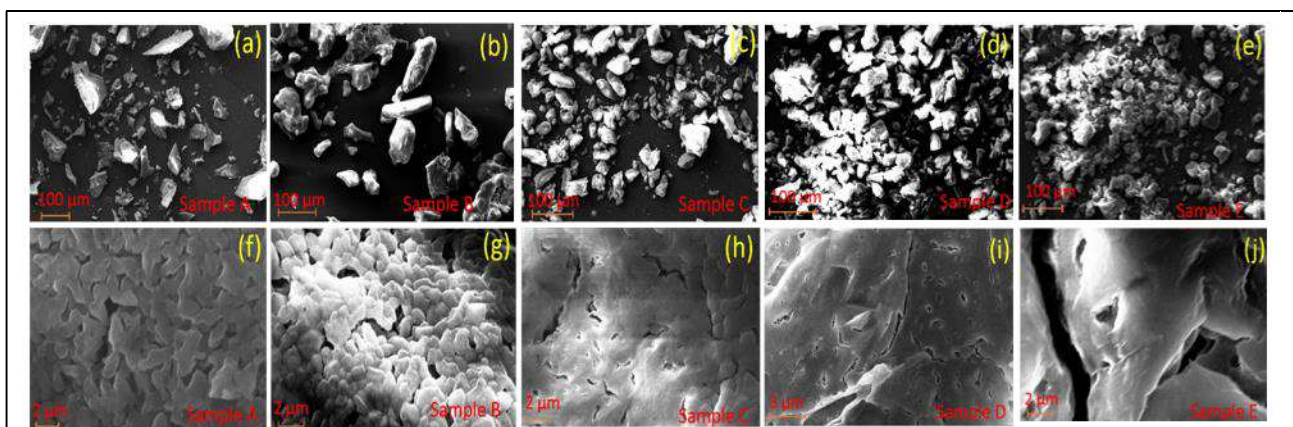


**Figure 6.3:** Scanning electron micrographs with 500 X (top panel) and 15000 X (bottom panel) magnifications for sample A, B, C, D and E.

## 6.3.4 Temperature-History Analysis

We carried out T-history measurements to measure thermal response of samples under investigation using an in-house built T-history set-up, as discussed in Chapter 3 and 4 [Kumar *et al.*, 2016 and 2017].

The deionized (DI) water is used as a reference sample. All PCM samples and deionized water are collected in glass test tubes. The weight of each sample is kept constant (~ 50 g) for respective T-history measurements. The physical properties of glass test tubes, all PCMs and reference samples, used for these measurements, are listed in Table 1.

**Table 6.1:** Physical properties of test tubes, PCMs and DI water used for experiments

| Sample name | Sample details | mass of test tube (g) | mass of sample material (g) | Specific heat of test tube (kJ.kg$^{-1}$. K$^{-1}$) |
|---|---|---|---|---|
| Reference | Deionized water | 28.057 | 50 | 0.84 |
| A | 94 wt% SAT + 6 wt% DI water | 28.123 | 50 | 0.84 |
| B | Sample A + 2 wt% EG | 28.427 | 50 | 0.84 |
| C | Sample A + 3 wt% EG | 28.235 | 50 | 0.84 |
| D | Sample A + 5 wt% EG | 28.326 | 50 | 0.84 |
| E | Sample A + 7 wt% EG | 28.148 | 50 | 0.84 |
| F | Sample A+ 10 wt% EG | 28.445 | 50g | 0.84 |

These samples are heated up to 80 °C inside the chamber to carry out temperature versus time (T-history) measurements and data is recorded at every 10 seconds time interval. The sample containers (here glass test tubes) are kept inside 150 mm diameter and 280 mm height cylindrical

expanded polypropylene (EPP) thermal insulations. The water T-history measurements are carried out to estimate the heat loss coefficients, as discussed in Chapter 4. The details about these measurements and the mathematical procedure are discussed by Kumar *et al.* 2017. The estimated values of heat loss coefficients $k_0$, $k_1$ and $k_2$ are -0.0425 W, 0.03252 W K$^{-1}$ and 2.8363 x 10 $^{-4}$ W K$^{-2}$, respectively.

The respective T-history measurements are carried out for aqueous SAT and SAT-EG composite samples A, B, C, D, E and F samples. The sample weights, insulation, positioning of k type thermocouples and ambient temperature conditions are kept identical during the measurements as that for water T-history measurements. The cooling T-history data has been recorded from 70 °C to ~30 °C with external nucleation in liquid samples at ~60 °C using solid SAT powder. The measured data are summarized in Figure 6.4(a), with the respective ambient temperature.
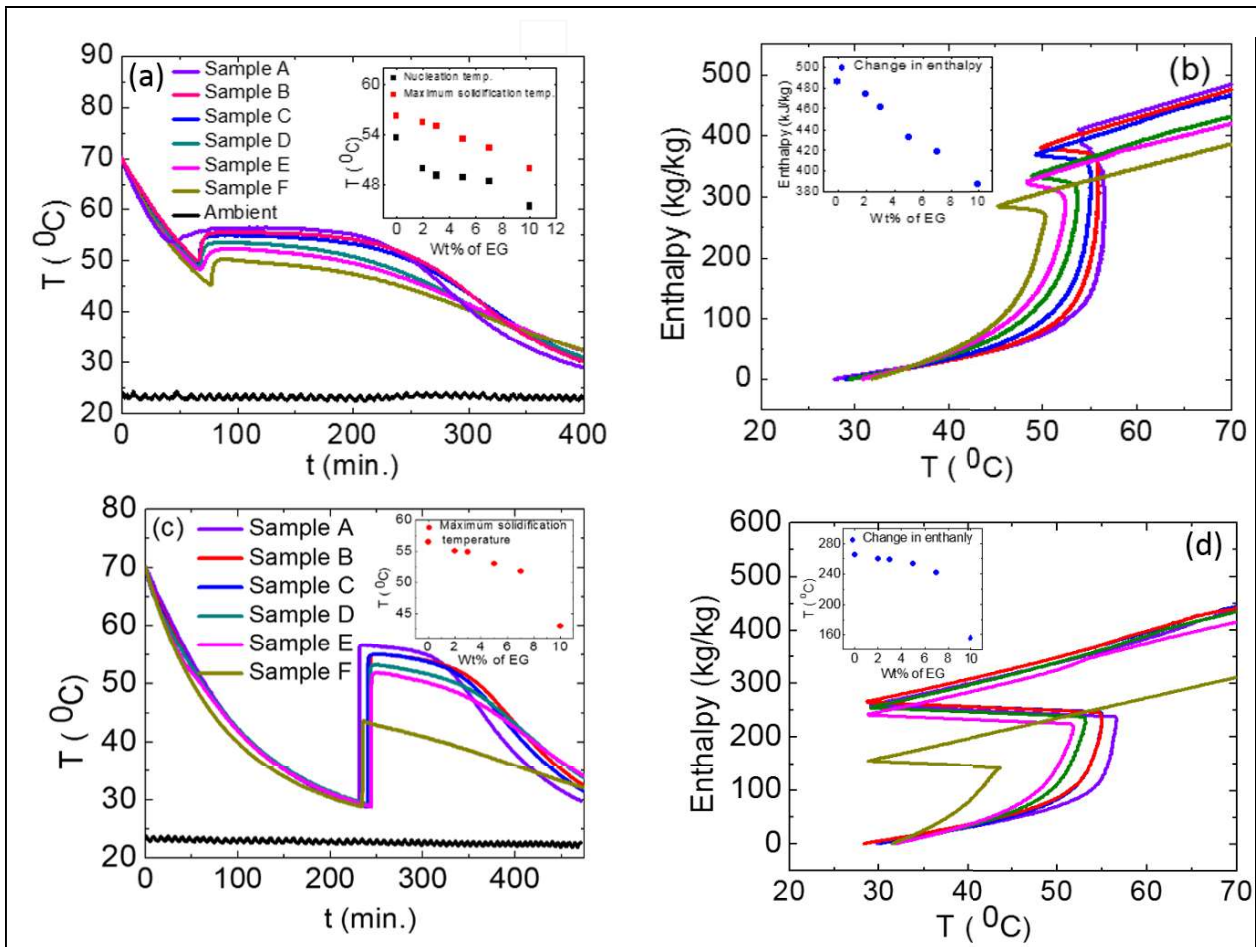


**Figure 6.4:** (a) T-history graphs for samples A, B, C, D, E and F nucleated at 60 °C and ambient temperature ~23 °C, (b) Enthalpy vs. temperature curves corresponding to graph 6.4(a), (c) T-history graphs for samples A, B, C, D, E and F nucleated at ~30 °C and ambient temperature ~23 °C, (d) Enthalpy vs. temperature curve corresponding to graph 6.4(c).

The temperature of sample A is exhibiting undercooling up to 53.6 °C and after that nucleation started in supercooled SAT liquid, which led to instant rise in temperature up to 56.6 °C. Samples B, C, D, E and F have shown enhanced supercooling temperature up to 49.9 °C, 49.1 °C, 48.9

ºC, 48.4 ºC and 45.4 ºC respectively, as explained in inset of Figure 6.4 (a). These observations suggest the enhancement in the degree of supercooling for SAT-EG composite samples with increasing wt% of EG. Thus, SAT-EG composite samples may exhibit better stability against spontaneous nucleation in metastable supercooled liquid state with respect to SAT sample. In addition, the maximum temperature achieved during solidification (heat releasing temperature) of SAT shows decrease with increasing wt% of EG and the maximum reduction has been observed for 10 wt% EG in SAT composite sample, as explained in inset of Figure 6.4 (a). These studies provide an avenue where variation of wt% of EG can be used as a parameter to tailor the heat releasing temperature and degree of supercooling of SAT PCM required for different applications. The first order derivatives of T-history measurements, not shown here, are used to find out completion of liquid-solid phase transformation temperature more accurately. The temperature corresponding to the completion of liquid-solid phase transformation decreases with increasing wt% fraction of EG i.e. the temperature range of liquid to solid phase transformation has increased with increasing wt% EG. The samples B and C take ~10% excess time to cool from 70 ºC to 40 ºC as compared to the sample A (SAT) for the same temperature range. This suggests that 2-3 wt% EG modified SAT samples (sample B and C) may provide thermal energy for longer time durations, thus more suitable for heat pack applications. However, samples with higher wt% EG in SAT (samples D, E and F) showed nearly same time as that SAT (sample A) for cooling from 70 ºC to 40 ºC temperature range. This is attributed to the reduction in respective enthalpies with increase in wt% EG, as observed in Figure 6.4(b).

These temperature versus time measurements in conjunction with the calculated heat loss coefficients $k_0$, $k_1$ and $k_2$ for deionized water are used to calculate the combined rate of heat loss from PCM and test tubes containing PCM samples, using following Eq. (6.1):

$$\dot{q}_{PCM+test\ tube,i} = k_0 + k_1\left(T_{PCM,i} - T_{amb,i}\right) + k_2\left(T_{PCM,i} - T_{amb,i}\right)^2 \tag{6.1}$$

The rate of heat loss from PCM has been calculated using following Eq. (6.2):

$$\dot{q}_{PCM,i} = \dot{q}_{PCM+test\ tube,i} + \left(m_t C_{pt}\right)\frac{\left(T_{PCM,i+1} - T_{PCM,i}\right)}{\left(t_{i+1} - t_i\right)} \tag{6.2}$$

where $\dot{q}_{PCM+test\ tube,i}$ and $\dot{q}_{PCM,i}$ are the rate of heat loss from PCM and test tube and the rate of heat loss from PCM at ith time interval, $m_t$ mass of test tube, $c_{p,t}$ constant pressure specific heat capacity of test tube (0.84 kJ kg$^{-1}$ K$^{-1}$), $T_{PCM,i+1} - T_{PCM,i}$ temperature difference between two consecutive measurements of PCM and $t_{i+1} - t_i$ is time interval between two consecutive measurements, which is 10 seconds for these measurements. The calculated rate of heat loss from PCM using Eq. (6.2) is used to calculate the change in enthalpy ($\Delta H_{PCM,i}$) of PCM for ith time interval using following Eq. (6.3)

$$\Delta H_{PCM,i}\left(T_{PCM,i}\right) = \frac{\dot{q}_{PCM,i}\ \Delta t_i}{m_{PCM}} \tag{6.3}$$

The calculated $\Delta H_{PCM,i}$ are summed to calculate the cumulative enthalpy of PCM samples with respect to the temperature. The calculated cumulative enthalpy versus temperature graphs are plotted in Figure 6.4(b). The cumulative enthalpies are plotted as an inset in Figure 6.4(b), for A, B, C, D and E and F samples at temperature 70 ºC nucleated at 60 ºC , suggesting that the enthalpy of sample A decreases with increasing wt% of EG in SAT. These results are consistent with the expected

reduction because of reduced fraction of aqueous SAT in aqueous SAT-EG composite phase change materials.

Additional T-history measurements are carried out for these samples, which are supercooled up to 30 °C and nucleated at this temperature using SAT fine powder. The measured T-history data are plotted in Figure 6.4(c). A sharp increase in temperature has been observed for all these samples after external nucleation. This rise in temperature is a consequence of latent heat release while solidification. This temperature rise has been summarized in the inset of Figure 6.4(c), suggesting decrease in temperature rise with increasing wt% of EG. This observation is consistent with that of observed while nucleating at 60 °C (inset Figure 6.4(a)). Inset in Figure 6.4(c) suggests that the heat releasing temperature can be tailored from 57 to 43 °C by simply varying wt% of EG up to 10%. The respective enthalpy versus temperature data are calculated as explained above and the results are plotted in Figure 6.4(d). The enthalpies of these samples at 30 °C against wt% EG are plotted as an inset in Figure 6.4(d). The enthalpies of these samples (nucleated at 30 °C) are lower as compared to that of samples, nucleated at 60 °C. The lower enthalpy values for samples, nucleated at 30 °C is mainly due to loss of thermal energy in the form of specific heat of liquid during cooling of PCM from 70 to 30 °C.

### 6.3.5 Differential Scanning Calorimetric Analysis

Further, thermophysical properties of these phase change materials are substantiated by Differential Scanning Calorimetric (DSC) measurements using DSC TA Q10 (TA Instruments USA make). The measuring sample is hermetically sealed in an aluminum pan and empty aluminum pan is used simultaneously as a reference sample. The instrument is calibrated using indium reference material before carrying out DSC measurements on these samples. The weights of sample A, B, C, D and E used for DSC measurements are 5.19 mg, 5.12, 5.86, 6.27 and 6.08 mg, respectively. The measurements are carried out at identical heating and cooling rate of 2 °C min$^{-1}$ under inert environment using continuous purging of nitrogen gas at 50 ml min$^{-1}$ flow rate. The melting and solidification of PCM samples are identified as endothermic (down) and exothermic peaks (up) in DSC thermographs shown in Figure 6.5 (a & b).
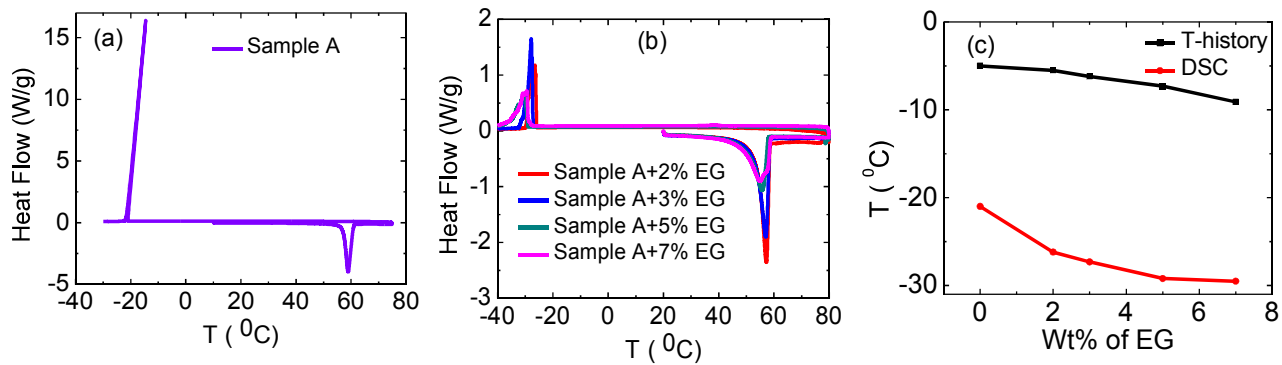


**Figure 6.5:** Differential scanning calorimetric (DSC) thermograph for sample A (a); samples B, C, D, and E (b) and supercooling temperature for these samples, measured using DSC and T-history methods (c)

Sample A exhibited sharp (narrow temperature window) endothermic and exothermic DSC peaks, as shown in Figure 6.5 (a). In contrast to sample A, EG modified composite PCM (samples B, C, D and E) showed wider endothermic and exothermic DSC peaks, Figure 6.5(b). The narrow temperature range of exothermic peak for sample A suggests a high rate of heat release in narrow

temperature window as compared to EG modified composite PCM samples. The onset and endset temperatures and latent heat of fusion for these PCM samples are estimated using DSC thermographs, Figure 6.5 (a and b), and results are summarized in Table 6.2. The observations are consistent with T-history observations, suggesting that melting/solidification temperature decreases and melting/solidification temperature range increases with increasing wt% of EG in aqueous SAT. The self-nucleating temperature of aqueous SAT decreases with increasing wt% of EG, suggesting enhancement in the degree of supercooling and thermal stability of metastable supercooled liquid against spontaneous nucleation.

**Table 6.2:** Melting and solidification temperatures of SAT and SAT+EG composite PCMs

| Sample Name | Onset temperature for melting peak of DSC (°C) | Endset temperature for melting peak of DSC (°C) | Onset temperature for solidification peak of DSC (°C) | Endset temperature for solidification peak of DSC (°C) |
|---|---|---|---|---|
| SAT | 57.6 | 60.1 | -21.0 | -21.68 |
| SAT + 2% EG | 54.3 | 58.2 | -26.2 | -29.2 |
| SAT + 3% EG | 53.5 | 57.8 | -27.3 | -31.8 |
| SAT + 5% EG | 49.5 | 56.8 | -29.2 | -37.0 |
| SAT + 7% EG | 47.8 | 55.8 | -29.5 | -38.1 |

The measured degree of supercooling for samples A, B, C, D and E using both DSC and T-history methods are plotted in Figure 6.5(c). This suggests that the degree of supercooling has enhanced for EG modified composite PCM samples. The values of self-nucleating temperatures for all samples measured with DSC are lower, as compared to that from T-history measurements. The difference in these results is attributed to the variation in sample mass, used for these measurements. In DSC, a very small amount (few milligrams) of the sample is being used for the measurements, which reduces the probability of nucleation as compared to that of the voluminous sample (few tens of grams), used in T-history measurements. Hence, T-history measurement values may be more reliable as compared to that of DSC measurements, for any real application, where usually large quantities of samples are used.

### 6.3.6 Microscopic Explanation of SAT-EG Interaction

The proposed atomic/molecular interaction between SAT and EG is shown schematically in Figure 6.6, based on vibrational spectroscopic results, inferred from FTIR measurements. The schematic molecular structure of SAT and EG are shown in Figure 6.6(a) and (b), respectively. The metastable supercooled liquid SAT solidifies in large and lumped continuous crystallites, as shown schematically in Figure 6.6(c). Such large lumped crystallites are not suitable for thermal heat pack applications. This can be mitigated by using the physical mixing of EG in SAT matrix. Here, EG is dispersed homogeneously in SAT matrix because of weak hydrogen bond interaction between SAT water hydrogen atoms and EG hydroxyl oxygen atoms, as observed and inferred from FTIR spectra of SAT-EG composite samples. The interaction mechanism is explained schematically in Figure 6.6(d). The uniform dispersion of EG assists in the adsorption of liquid EG layers on the growing SAT crystal faces. Thus, these liquid EG layers inhibits the growth of large and lumped SAT crystallites. This liquid EG forms the laminar vesicles, as observed in microscopic studies, Figure 6.3.

(a)

(b)

(c)

(e)

(d)
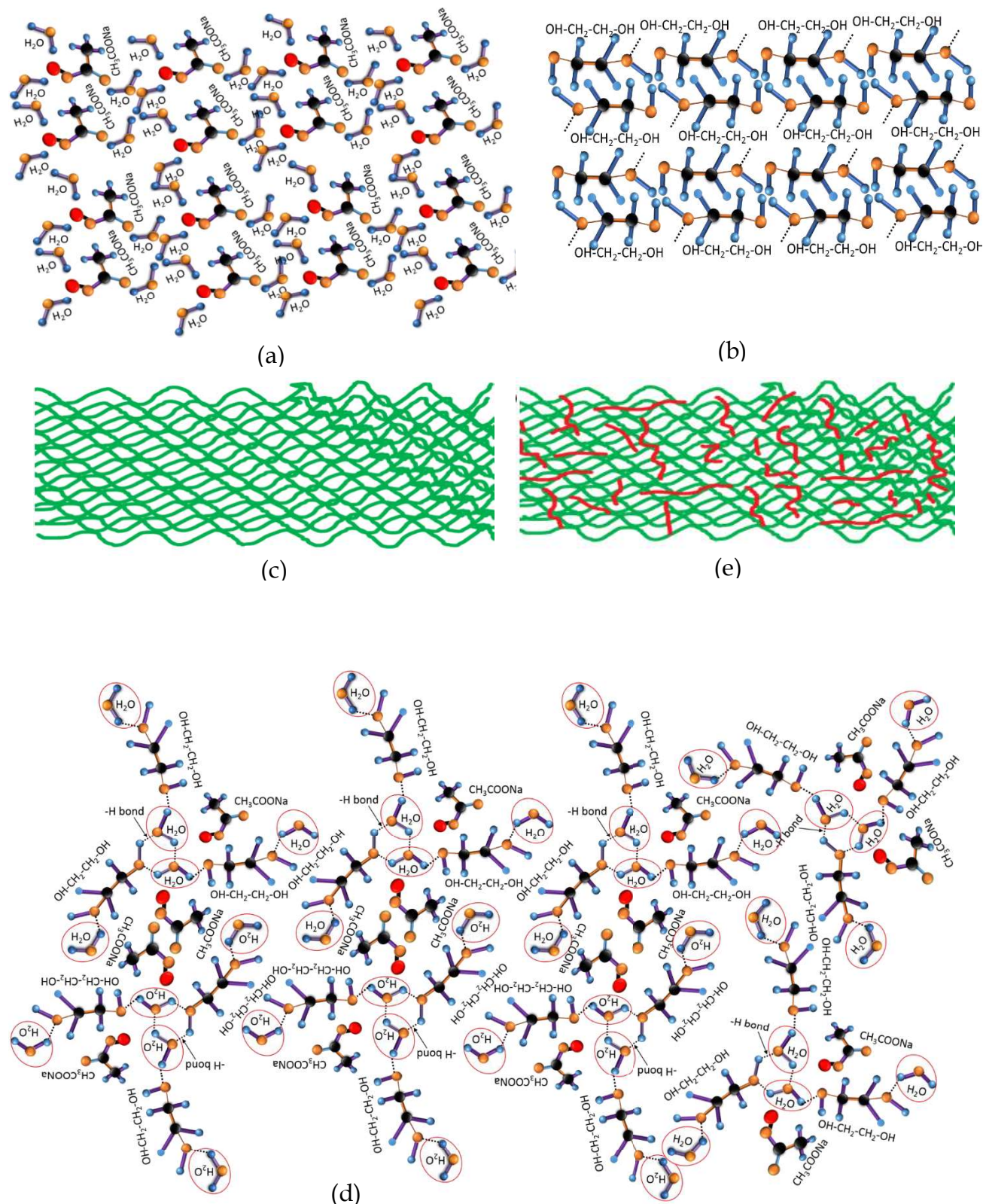
**Figure 6.6**. Schematic representation of SAT molecules (a), EG molecules (b), macroscopic arrangement of SAT crystals (c), hydrogen bond interactions between water H atoms of SAT and hydroxyl oxygens of EG (d), and macroscopic arrangement for insertion of EG as laminar vesicles (red lines) in SAT matrix (e). The blue, black, yellow and red spheres represent the H, C, O and Na atoms respectively. The hydrogen bond between hydrogen atom of water and hydroxyl atom of EG is represented with doted black lines

The process of laminar vesicles formation in SAT is explained schematically in Figure 6.6(d). These laminar vesicles of liquid EG in SAT crystals are responsible for weakening the SAT crystallites and thus, reducing the continuous growth of SAT crystallites. Further, this inculcated liquid EG will assist in softening, by breaking crystallites with external stimuli causing shear forces between EG separated SAT planes, as shown schematically in Figure 6.6(e). The hydrogen bonding between ethylene glycol and $H_2O$ molecules of SAT may disturbs the hydrogen bonding between SAT and $H_2O$ molecules. It may be the responsible for enhancement of activation energy required to form nuclei with critical radius and enhances the degree of supercooling and thermal stability of SAT-EG metastable supercooled liquid PCM against spontaneous nucleation compared to SAT.

Thus, ethylene glycol and aqueous sodium acetate trihydrate composite phase change materials with enhanced thermophysical properties have been designed and developed for different thermal applications. Thermophysical properties of aqueous SAT PCM, such as melting/solidification temperatures, degree of supercooling, heat retention/release time, have been tailored and optimized by varying EG weight fraction in aqueous SAT-EG composite phase change materials for specific applications. The optimal ~10% enhancement in heat retention time has been observed for 3 wt% EG modified aqueous SAT PCM, without affecting other thermophysical properties significantly. The thermal stability of metastable supercooled liquid SAT against spontaneous nucleation has enhanced significantly for aqueous SAT-EG composite PCMs. In addition, the insertion of liquid EG into SAT crystallites helps in controlling the SAT crystallites size by hindering the growth of large and lumped SAT crystallites. The thermal response of developed aqueous SAT- EG composite PCMs has shown promising thermophysical properties for possible applications such as therapeutic/body warming, building heating under adverse conditions and seasonal solar thermal energy storage. These studies suggest that aqueous SAT-EG composite PCM may improve the flexibility and physical stability of PCM heat packs for the desired applications.

### 6.3.7 Fabrication and Evaluation of PCM Heat Packs
Sample C (aqueous SAT with 3 wt% EG) is used for fabricating PCM heat packs because of its relatively superior thermophysical properties as discussed and explained in earlier sections. Three heat packs, containing 300 g water, sample A and sample C, are fabricated to compare the thermal performance. Polyvinyl chloride (PVC) has been used as a packaging material for storing PCM in conjunction with a triggering device. The stainless-steel triggering device, consisting surface imperfections, is kept inside PCM packs to release heat at the time of requirement. The actual photograph and schematic of such fabricated heat pack (110 mm x 180 mm) and solidification mechanism in PCM heat packs is explained in Figure 6.7 (a - c). The triggering device is flexed to start nucleation for solidification of PCM in heat packs, Figure 6.7 (a). This solidification propagates in all the three directions, Figure 6.7 (b) and takes about one minute for complete solidification of PCM, Figure 6.7 (c). The thermal energy equivalent to the latent heat of PCM is released during this process.
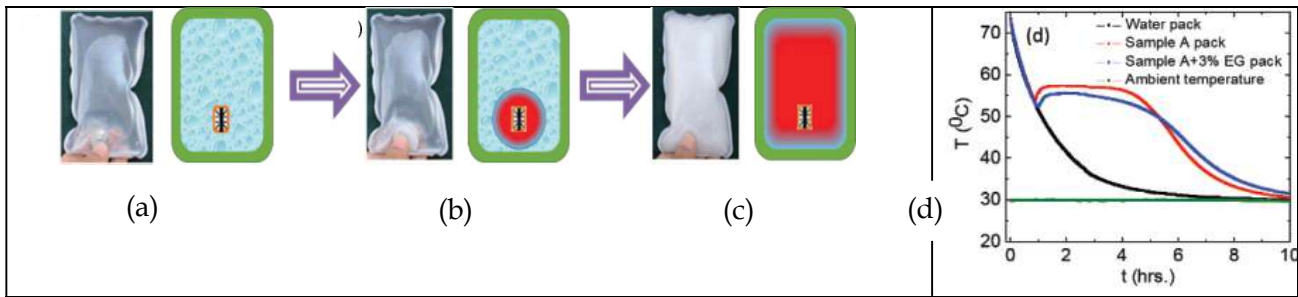
**Figure 6.7.** Schematic and pictorial representation of heat releasing process from PCM heat packs: (a) flexing triggering device to start nucleation in supercooled liquid PCM for its solidification at t=0 second, (b) growth of solidification at t=5 seconds, (c) complete solidification of supercooled liquid PCM at t= 55 seconds and (d) T-history curves for heat packs consisting of water, sample A and C.

The heat packs are kept inside an insulated box (size 150 mm x 220 mm x 10 mm) made of 20 mm thick EPP material, to ensure thermal equilibrium across the heat pack during T-history measurements. This insulated box is kept inside T-history heating-cooling chamber and heat packs are heated up to 80 °C, followed by cooling up to ambient temperature ~30 °C. The thermal response of these heat packs is recorded from 75 to 30 °C at every 10 seconds time interval. The PCM inside the heat packs is nucleated at 60 °C above its melting temperature. The measured T-history responses of these three packs are plotted in Figure 6.7 (d). Water, sample A and C based heat packs took about 2.24, 6.40 and 7.03 hours, respectively to cool from 75 to 40 °C temperature. Thus, extended heating time for heat packs containing sample A and C is about 186% and 214% more as compared to the water heat pack. Further, an enhancement of ~10% additional heat release time has been observed for sample C based heat pack with respect to sample A based heat pack.

## 6.4 CONCLUDING REMARKS

Novel ethylene glycol and sodium acetate trihydrate composite phase change materials with enhanced thermophysical properties are designed and developed for different thermal applications. SAT thermophysical properties such as melting/solidification temperatures, degree of supercooling, heat retention/release time are tailored and optimized by varying EG weight fraction in SAT-EG composite phase change materials for specific applications. A composite sample with 3 wt% ethylene glycol has shown the optimal ~10% enhancement in heat retention time without affecting other thermophysical properties significantly. The thermal stability of metastable supercooled liquid SAT against spontaneous nucleation has enhanced significantly for ethylene glycol-SAT composite PCMs. In addition, the insertion of ethylene glycol into SAT crystallites helps in controlling the SAT crystallites size by hindering the growth of large and lumped SAT crystallites. The thermal response of developed SAT-ethylene glycol composite PCMs showed promising thermophysical properties for possible applications such as therapeutic/body warming, building heating under adverse conditions and seasonal solar thermal energy storage. These studies suggest that SAT-EG composite PCM may improve the flexibility and physical stability of PCM heat packs for the desired applications

...